



# HAR-sEMG: A Dataset for Human Activity Recognition on Lower-Limb sEMG

Yu Luan<sup>1</sup> · Yuhang Shi<sup>3</sup> · Wanyin Wu<sup>4</sup> · Zhiyao Liu<sup>1</sup> · Hai Chang<sup>1</sup> · Jun Cheng<sup>2,5</sup>

Received: 11 July 2020 / Revised: 8 July 2021 / Accepted: 11 July 2021 /

Published online: 7 September 2021

© The Author(s), under exclusive licence to Springer-Verlag London Ltd., part of Springer Nature 2021

## Abstract

In the past decade, human activity recognition (HAR) has grown in popularity due to its applications in security and entertainment. As recent years have witnessed the emergence of health care and exoskeleton robotics which make use of wearable suits, human–machine interaction based on action recognition performs an important role in multimedia applications. Considering the limitations of the application scenario, the surface electromyography (sEMG) signal stands out in many wearable data collection devices for HAR. That is because: (1) timely feedback; (2) no damage to the human body; and (3) the wide range of recognizable actions. However, existing public datasets of sEMG contained relatively few activities, and several large-scale datasets only collected the action of the hand. In addition, the processing of sEMG signals is a new field with no effective evaluation system for it. To tackle these problems, we establish a novel dataset for HAR on lower-limb sEMG named “HAR-sEMG,” using 6 sEMG signal sensors attached to the left leg. A benchmark summarizing experiments with many combinations of existing high-dimensional signal processing algorithms-based manifold learning on our dataset is also provided for a performance analysis.

**Keywords** Human activity recognition · Surface electromyography · Human–machine interaction · Wearable · benchmark

## 1 Introduction

The lower-limb activity recognition system based on sEMG is a hot spot in the field of human–computer interaction, including sEMG signal collection, preprocessing, feature extraction and motion recognition, so it can be regarded as an information process system [37]. With the development of information technology, information process systems can be seen everywhere. [12] proposed a deep model framework for predicting the price of second-hand products based on pictures and text descriptions. [60] proposed a method for learning sentence representation based on convolutional neural networks. In fact, above work belongs to information processing system. Human activity recognition (HAR) has received intensive attention in the field of health care [47], military [34], and security applications [2], such as hospital and nuclear power plant scenes. Generally, patients with diabetes or heart disease often need a regular exercise routine for their treatments. Therefore, recognizing their daily

Extended author information available on the last page of the article

activities is important for a caregiver to obtain the feedback about the behavior of a patient [9, 50]. Likewise, HAR can be used for daily behavioral monitoring of the elderly living alone. Besides, HAR is also a significant part of signal processing in exoskeleton robotics [58]. Generally, human activity recognition aims to identify the activities carried out by individuals through a set of data, such as pictures, signals from IMU or bioelectricity signals [18]. In recent years, many pattern recognition schemes have been introduced to resolve HAR problems. The existing human activity recognition methods, which can be divided into three categories: computer vision-based, acceleration-based, and surface electromyography (sEMG) signal-based methods. We reviewed some remarkable works as follows.

Computer vision-based methods for human action recognition mainly focus on detecting, tracking, understanding, and identifying the expression of person behaviors from image sequences. During the past years, various significant progresses based on computer vision have been made to resolve the human activity recognition task [23]. For example, Umakanthan et al. [51] proposed an effective feature representation method to address the shortcomings of the bag-of-words approach. Zhang et al. [59] improved the accuracy of action recognition by applying subspace clustering. Chaaraoui et al. [8] proposed an adaptive vision-based human action recognition method which extracted features from frames and projected the pose representation from videos. According to the skeletal representation, Vemulapalli et al. [52] constructed a kinematic model that clearly simulated the geometric relationship between different body parts. Käse et al. [25] proposed a method of human action recognition based on multi-view video, which used the temporal and spatial changes in continuous video frames to solve the problem of human activity recognition, and achieved good classification accuracy on i3dpost and ixmas datasets. However, computer vision-based methods are not always satisfactory [61], given the performance of action recognition can be affected by spatial and illumination changes, or body movement.

Acceleration-based human activity recognition is an alternative approach which has received intensive attention due to the wide application of smart mobile devices. It exploits the acceleration signals obtained from smart mobile devices [62] and recognizes general human activities such as running, walking downstairs, and jumping. This approach provides an innovative way to transfer the classification of human body activities into pervasive computing. Recently, Kwapisz et al. [29] utilized phone-based accelerometers to resolve the activity recognition task. Bonomi et al. [7] developed models for the detection of type, duration, and intensity of human physical activities using one accelerometer. Jalal et al. [22] presented novel features to classify actions based on triaxial accelerometry. Lee et al. [30] proposed a 1-D CNN framework to recognize activities by utilizing the accelerometer information obtained from the user's phone, so this approach acquired a more powerful recognition performance than the baseline random forest algorithm. Hernández et al. [19] proposed a human activity recognition system to combine accelerometer with gyroscope data as the inputs of a bidirectional long short-term memory (LSTM) network, and six related activities were recognized correctly. Nurhanim et al. [35] presented a multi-class support vector machine to classify human daily living activities such as laying, sitting, and walking downstairs. Lu et al. [32] proposed a triaxial accelerometry recognition framework using a modified recurrence plot, and comparison experiments showed its stronger robustness to noise signals and low decimation rate. In order to improve the accuracy of motion recognition method based on acceleration, a lot of acceleration sensors were used, which brought great difficulties to the calculation. Later, the research in this field gradually turned to the single accelerometer to realize the action recognition and achieved satisfactory accuracy.

Surface electromyography (sEMG) [13, 16] is one kind of weak biological electricity signals produced by muscle contraction during limb movement. Compared with computer

vision-based and acceleration-based methods, sEMG is not limited by the space and illumination conditions, and it can vividly reflect the characteristics of action with few sensors. Therefore, learning sEMG representations automatically from wearable sensors is deemed as a more significant strategy. Currently, sEMG signal-based method has played an increasingly prominent role in human activity recognition task. For instance, Wu et al. [55] proposed an SLR system to fusion sEMG at the feature level, and the results of recognition rate illustrated the effectiveness of the method. Wei et al. [53] proposed a multi-stream CNN framework to analyze surface electromyography signals; this framework, consisting of decomposition and fusion stages, was powerful for the classification of hand gestures. Xi et al. [56] investigated 15 feature extraction methods, such as the Wilson amplitude feature of sEMG signals, to tackle activity monitoring and fall detection problems. Szabó et al. [46] utilized the seizure detection algorithm to evaluate the patient sEMG signals, and related experiments validated the powerful sensitivity and specificity of the algorithm, so this algorithm can be applied to the automatic detection of generalized tonic–clonic seizures. Feng et al. [13] proposed a three-segment cavity structure to analyze the finite element of sEMG, and this algorithm provided significant theoretical support for human–robot interaction.

We have reviewed three kinds of action recognition methods, different scenes for human activity recognition use different data formats, such as video, sEMG signal. The advantage of vision-based method is that the test object does not need to wear any sensors, but the performance of this method depends on lighting conditions, perspective, and other external factors. On the contrary, the acceleration-based method and the sEMG-based method require the test object to wear sensors, but these two methods almost eliminate the influence of all external factors, only the noise of mains will affect collected data. In today's advanced filtering technology, these noises are easy to eliminate. Besides, sEMG signal is generated 30–150ms ahead of the action, so action can be predicted based on this characteristic, which is incomparable with the acceleration signal. In order to promote the study of sEMG action recognition of lower limbs, we propose HAR-sEMG dataset. In detail, our contributions can be summarized as follows: (1) We introduce the HAR-sEMG dataset to verify the effectiveness of human motion recognition based on sEMG, and this dataset can evaluate and advance the performance of new data-driven algorithms for human activity recognition; (2) we also propose an evaluation benchmark for our dataset, and the results can be reported as a useful baseline in terms of activity recognition performance, providing useful insights for this direction. The rest of this paper is arranged as follows. In Sects. 2 and 3, we will briefly present an overview of manifold learning methods and publicly available datasets on sEMG. In Sect. 4, we will detail the process of data collection, while the benchmark for our dataset will be described in Sect. 5. Section 5 also shows the experimental results and discussion on the HAR-sEMG dataset. And the conclusion of this paper will be given in Sect. 6.

## 2 An overview of manifold learning methods

In this section, we briefly summarized several manifold learning methods. PCA [54] uses linear projection to reduce data dimensionality, so that the projection of the data in a given direction can get the largest variance. When the manifold is linear, the results obtained by PCA are optimal, but PCA cannot effectively deal with nonlinear data. For data dimensionality reduction on nonlinear manifold, representative methods include LLE [40], LE [6], Isomap [48] and LPP [17]. LLE is a nonlinear dimensionality reduction algorithm, which can maintain the original manifold structure after dimensionality reduction. LLE is an algorithm

that uses local linearity to reflect global nonlinear characteristics and enables the reduced-dimensional data to maintain the original data topology. LE uses an undirected weighted graph to describe a manifold, finds the low-dimensional representation of data by embedding the graph, and maps the graph formed by manifold data from a high-dimensional space to a low-dimensional space while maintaining the local adjacency of the graph. Isomap uses the idea of geodesic in differential geometry to ensure the geodesic distance on the manifold can be maintained after data are mapped to a low-dimensional space. Intuitively, it is to maintain the relative distance between the data points before projecting the data into the low-dimensional space. The purpose of the LPP algorithm is to realize the learning and analysis of nonlinear manifolds. LPP can extract the most discriminative features for dimensionality reduction. It is a dimensionality reduction method that maintains local information and reduces many factors that affect data recognition. This algorithm is essentially a linear dimensionality reduction method. Because of its ingenious combination of the idea of LE, it can effectively maintain the nonlinearity of the data after dimensionality reduction.

### 3 An overview of existing sEMG datasets

In this section, we briefly summarized several publicly available sEMG datasets. A statistical summary of each dataset is listed in Table 1. The existing shared datasets in this field can be classified into three categories, namely hand movements, finger movements, and lower-limb movements. Furthermore, the datasets on hand movements account for the majority of these public datasets.

NinaPro dataset [5] is the benchmark repository with the highest number of intact and hand amputated identities. This dataset collects sEMG signals from the forearm and upper arm using 10–16 sEMG channels together with several recorded from 117 able-bodied identities and 13 amputees. It contains a partial set of 61 pre-defined hand and finger movements. Besides, the dataset is extracted from different sEMG acquisition device systems, including an Otto Bock MyoBock System for Ninapro 1 [4], a Delsys Trigno Wireless sEMG System for Ninapro 7 [28], a Cometa Wave Plus wireless sEMG system for Ninapro 4 [38]. As a result, there is no consensus on sampling rate, filtering, resolution, and gain. Therefore, some manipulation and transforming preprocessing are necessary before combining sEMG data from different Ninapro data sources.

Khushaba dataset is an enhanced dataset for it can be divided into 6 sub-datasets. Among the sub-datasets, dataset 1 [26] contains eight normally limbed identities. The above-required finger movements, including 2 channels and 10 classes, are performed by the recruited 6 males and 2 females all aged between 20 and 35 years. Compared with dataset 1, dataset 3 [27] identifies eight individuals and the fingers of the recruited participants are the pressure on a steering wheel. In contrast with the above sub-datasets, dataset 4 [3] improves the performance against force variation of sEMG, thus controlling the multi-functional upper limb prostheses for trans-radial amputees.

Sapsanis dataset is an alternative hand movement dataset. This dataset contains two different sub-datasets. Specifically, dataset 1 [43] consists of 5 healthy identities captured from 2 males and 3 females. During the hand movement data collection stage, each test is conducted as six grasps for 30 times, and the measure time is 6 sec. Dataset 2 [42] includes 1 healthy identity extracted from a 22-year-old male. The data collection is carried out by six grasps for 100 times during 3 consecutive days, and the measure time is 5 sec. The identities are required to perform repeatedly the following six movements: (a) holding spherical tools; (b)

**Table 1** An overview of existing open sEMG datasets. (S indicated the sound, A indicated the amputee, M indicated male, and F indicated female.)

Dataset	Year	Identities	Number of movement	Total number of trials	Location	Sampling frequency (Hz)	Interval collection?
Ninapro 1 [4]	2012	27S (20M 7F)	52	14040	hand; fingers	100	No
Ninapro 4 [38]	2017	10S (6M 4F)	52	3120		2000	No
Ninapro 7 [28]	2017	22 (20S 2A)	40	5280		2000	No
Khushaba 1 [26]	2012	8S (6M 2F)	10	480	fingers	4000	No
Khushaba 4 [3]	2015	11S (9M 2F)	7	2310	upper limb	4000	No
Sapsanis 1 [43]	2013	5S (2M 3F)	6	900	hand	500	No
Sapsanis 2 [42]	2013	1S	100	1800	hand	4000	Yes
Al-Timemy [3]	2016	9A (7M 2F)	6	1077	hand	2000	No
Theo [49]	2011	4S (3M 1F)	20	100	upper arms; upper legs	1000	No
BASAN [10]	2014	22S	3	132	lower limb	1000	No
<b>HAR-sEMG</b>	<b>2020</b>	<b>9S (7M 2F)</b>	<b>5</b>	<b>3600</b>	<b>lower limb</b>	<b>2000</b>	<b>Yes</b>

**Table 2** The summary of lower-limb sEMG dataset

Action	Dataset
Running	HHMM [12], PDR [36], HAR-sEMG
Standing	SUKFNN [57], TAS [15], HAR-sEMG
Lunge Stretching	HAR-sEMG
Jumping	HHMM [12], HAR-sEMG
Walking	HHMM [12], PDR [36], SUKFNN [57], TAS [15], HAR-sEMG

holding small tools; (c) grasping with the palm facing the object; (d) holding thin and flat objects; (e) holding cylindrical tools; and (f) supporting a heavy load.

BASAN dataset [10] contains 22 male identities, with half of them diagnosed with different knee abnormalities. In the data collection stage, all the participants undergo three movements, including sitting, standing, and walking, for the purpose of analyzing the behavior associated with the knee muscle, gait, leg extension from a sitting position, and flexion of the leg up. Besides, the data acquisition process is conducted with 4 electrodes, including vastus medialis, semitendinosus, biceps femoris and rectus femoris, and the goniometer in the knee.

Theo dataset [3] is collected by Theodoridis University. To measure the human activity, they choose 3 males and 1 female to perform the experiment. Throughout the 20 individual experiments, each identity of the experiments contains 10 normal and 10 aggressive activities, and the performance of the identity is recorded by Delsys sEMG apparatus. Based on the above context, the data acquisition process involves 8 skin-surface electrodes placed on the upper arms and upper legs, or more specifically, on biceps, triceps, thighs, and hamstrings.

The HHMM dataset [36] collected the sEMG signals of the lower limbs from five subjects, including walking, running, jumping, and sitting. The MFWF dataset [57] collected a total of 600 sEMG signals of the lower limbs from 5 subjects, including four movements of upstairs, downstairs, uphill, and downhill. The PDR dataset [15] collected the sEMG signals from 5 subjects, including walking, upstairs, downstairs, and running. The SUKFNN dataset [45] collected a total of 2500 sEMG data from 5 subjects. The collected actions included walking, crossing obstacles, standing, downstairs, and upstairs. The TAS dataset [41] collected the sEMG data of five kinds of actions from 10 subjects: walking, sitting, standing, going upstairs, and going downstairs. Besides, some datasets for lower limbs are only partially available online, which requires contacting the researchers who shared the data to access a full dataset, such as Jung et al. [24] who introduced a dataset for exoskeleton robots. To the best knowledge of us, there have been few public sEMG datasets on lower-limb movements until now, and the types of movements involved are not comprehensive. Table 2 shows those datasets sorted by actions.

As mentioned above, we proposed an HAR dataset for lower-limb movements on sEMG, called HAR-sEMG in Table 1, which contained more real and dynamic movements, including running, standing, lunge stretching, and walking. More real means that our dataset is collected in the natural environment. All actions are not trained in advance. The collected signals go through the process of skin drying to sweating, which simulates the whole process of human movement, so it is more real. Remarkably, considering that human sEMG signals fluctuate at different times, we also collected sEMG in different periods. Hopefully, the creation of this dataset will enable other researchers to improve the reliability and reproducibility of experiments on sEMG and reduce the costs of research.

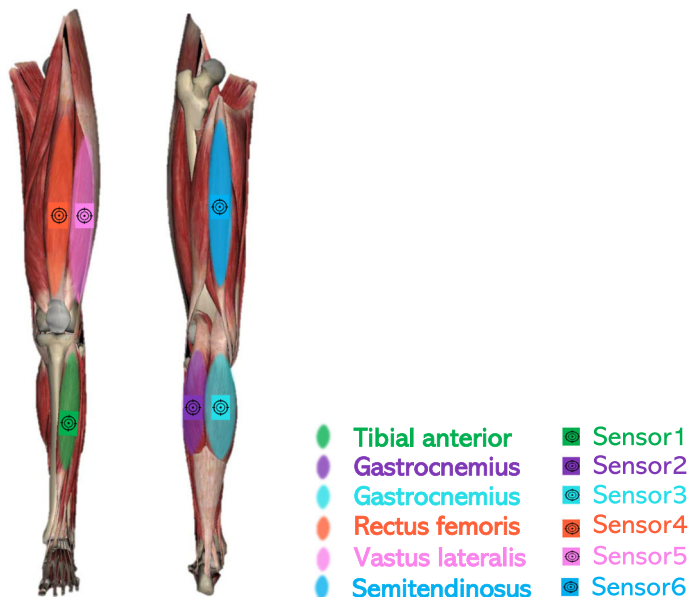


**Fig. 1** Placement of sensors on the left leg

#### 4 HAR-SEMG dataset

We selected 6 key muscles that drive lower-limb movements and are highly recognizable in the muscle group. Correspondingly, 6 sensors, which were attached to 6 muscle positions, respectively, recorded sEMG signals in the HAR-sEMG dataset. And they were sequentially placed on the tibialis anterior, gastrocnemius muscles of the left calf, the rectus femoris, vastus lateral femoral, and semitendinosus of the thigh, as shown in Fig. 1, where the muscle map was drawn by 3D body software [21].

HAR-sEMG utilized Trigno wireless biofeedback sensors to collect signals. The sEMG is a continuous signal and cannot be directly processed by a computer, so it needs to be converted into a discrete signal. The sampling frequency affects the quality of the discrete signal, the higher the sampling frequency, the closer the discrete signal is to the continuous signal. The equipment we selected provides two sampling rates of 1000 Hz and 2000 Hz. In order to ensure the quality of the data, we select a sampling rate of 2000 Hz.

A total of 9 healthy volunteers (7 males and 2 females) at an average age of 23.5 participated in the collection of the HAR-sEMG dataset, providing 1800 signals, each with a duration of 10 s. When collecting the sEMG signal of the volunteer, the volunteer was asked to wipe the skin where the sensor was attached with alcohol cotton to reduce the influence of sweat and oil on the skin surface. In addition, all volunteers were asked to perform 4 required movements that belong to the most frequent human movements (running, standing, walking, jumping) in daily life and without additional time for training. In order to prevent muscle strain, we asked the volunteers to do lunge stretching to warm-up, we additionally collected the sEMG signal of the lunge stretching, each action is repeated 20 times, and the explanations and description of different movements are listed in Table 3. The frequency and speed of activities were collected according to the activity habits of volunteers, respectively. Therefore, sEMG from different volunteers exhibited different fluctuation periods, which

**Table 3** Definition of the five movements

Movements	Definition
Running	Jogging for 10 s
Standing	Standing & doing nothing
Lunge Stretching	Pressing the left leg at normal rhythm for 10 s
Walking	Walking for 10 s at normal speed
Jumping	Jumping for 10 s without advancing

**Table 4** Statistical information of HAR-sEMG dataset

Identities	Number of Movement	Collection Times of Each Movement	Duration of Each Sample	Sampling Frequency
9S (7M 2F)	5	40	10 s	2000 Hz

would increase the difficulty of recognition but would be closer to the real-world activities at the same time. The collected original signal also needs to be denoised, leaving a clean signal for subsequent use. Knowing that the useful signal frequency of the sEMG signal is 0–500Hz, we use a band-pass filter to extract this part of the useful information. In addition, the sEMG signal is also affected by the 50/60Hz noise from the mains, and we use a notch filter to filter this noise. Table 4 lists the statistical information of HAR-sEMG dataset.

Notably, the sEMG is not always the same when each person does the same movement, so we collect the signal twice for each volunteer, the time interval is 24 h, and the error is not more than 30 min. Each data were composed of 6 channels of sEMG signals. In addition, to expand the size of samples, we split the original signal into two segments, and the duration of each signal was 5 s, thereby increasing the number of datasets to 3600. Figure 2 shows different classes of lower-limb movements in 10 s, and from top to bottom were the corresponding signals captured by sensor channel 1 to 6, respectively, the left side is the sEMG time domain signal, and the right side is the sEMG frequency domain signal. It can be seen from Fig. 2 left side that the sEMG signals of running and walking are very similar, but because the interval of running action is shorter than walking, the sEMG signal peak in the running state appears more frequently. In the standing state, the 6 sensors all showed continuous and obvious sEMG signals, and it can be seen that the 6 selected muscles are all exerting force when standing. All sensors have regular waveforms in the state of lunge stretching. The sEMG signal generated by continuous jumping is shown in Fig. 2e. It can be seen that the muscles corresponding to the six sensors are involved in the jumping movement. Compared with running and walking, the regularity and wave peak are more obvious. As shown in Fig. 2 right side, the sEMG signal is converted to the frequency domain, and the data are normalized. It can be seen that no matter what kind of action, the spectrum distribution of the useful signal of sEMG is between 0 and 500 hz, and the energy is mainly concentrated between 0 and 150 hz, which fully reflects the low-frequency characteristic of sEMG signal.

## 5 Benchmark evaluation of HAR on HAR-SEMG

Next, we provided a scheme on the proposed dataset to conduct human activity recognition based on dimensionality reduction algorithms, given the high dimension and high noise of

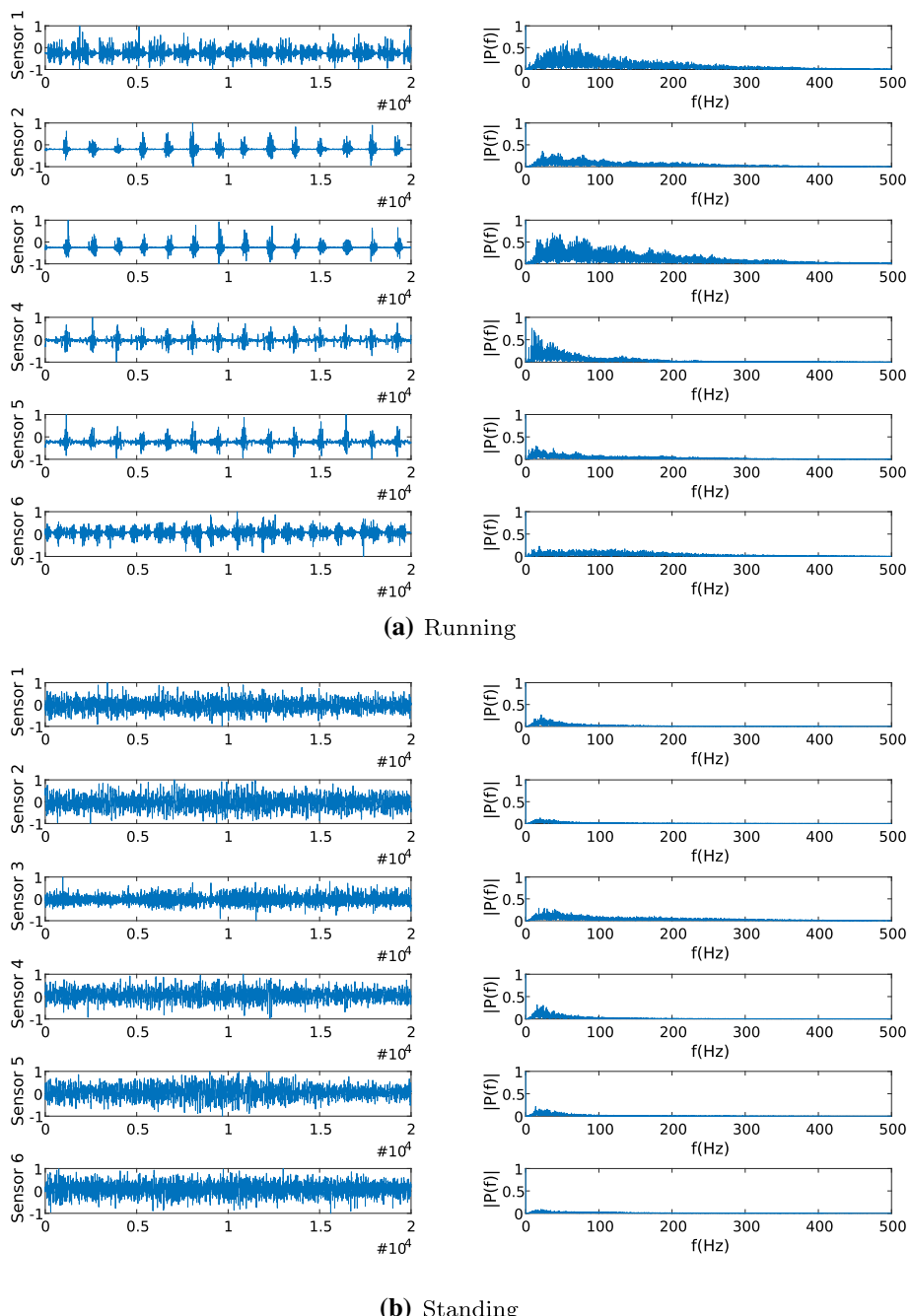
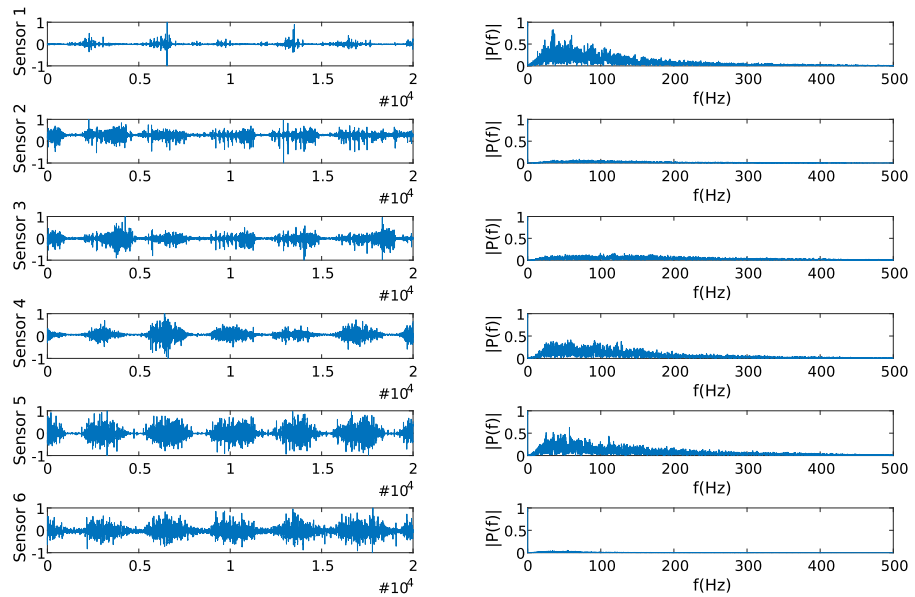
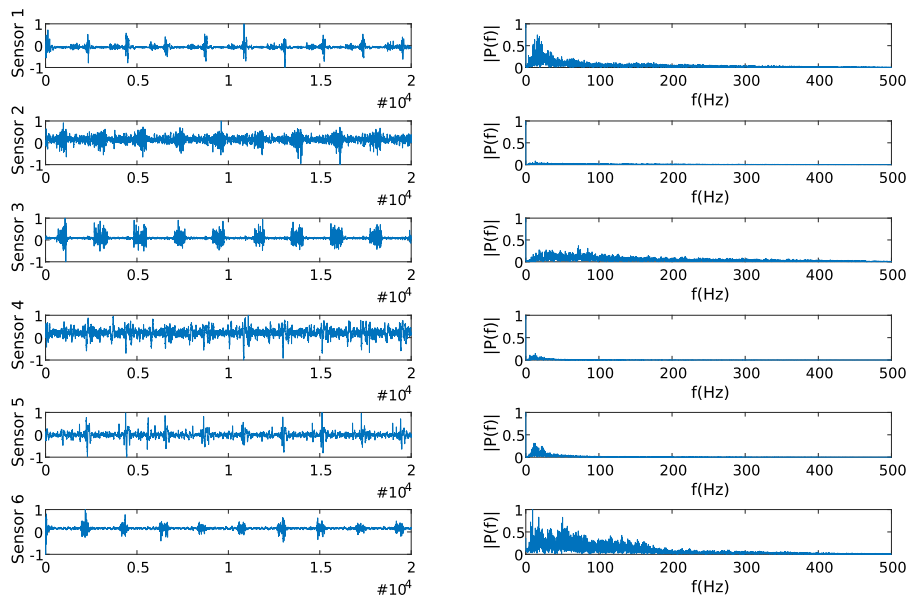


**Fig. 2** Examples of sEMG signals for five movements in 10 s

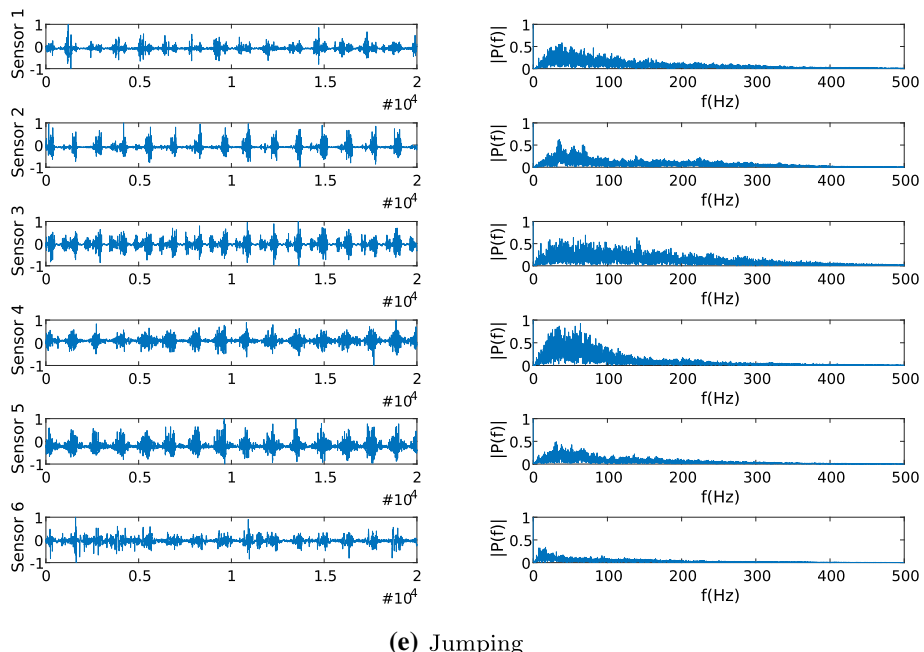


(c) Lunge Stretching



(d) Walking

**Fig. 2** continued



(e) Jumping

Fig. 2 continued

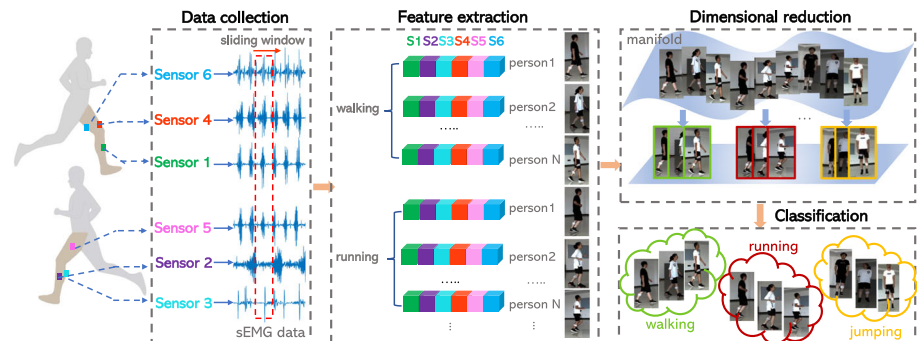


Fig. 3 Framework of human activity recognition system on lower limb sEMG

sEMG signals. The program framework is shown in Fig. 3. We presented the details of our systematic experimental evaluation of 5 existing dimensionality reduction algorithms for sEMG signal processing, producing an up-to-date benchmark on the HAR-sEMG dataset. The different dimensionality reduction algorithms from our evaluation system were summarized below firstly.

## 5.1 Dimensionality reduction

Many practical applications of sEMG involve large volumes of high-dimensional data. In the past decades, unlimited significant efforts have been made to exploit meaningful low-

dimensional structures hidden in the high-dimensional observations. According to whether the local neighborhood relationship is calculated or not, those algorithms can be divided into global dimensionality reduction and local dimensionality reduction.

### 5.1.1 Global dimensionality reduction

Global dimensionality reduction considers the correlated data as a whole and reduces them to a suitable low dimension. Here we cited several classic global dimensionality reduction methods, which are widely used in sEMG.

(1) **Principal component analysis (PCA)** [54] aims to seek the low-dimensional subspace principle to linearly represent the high-dimensional raw data that preserve the main initial information. Assuming a given sample set  $X = [x_1, x_2, \dots, x_k], x_i \in R^D$  the orthogonal unit vectors  $V = \{v_1, v_2, \dots, v_l\}$  work as the basis of a low-dimensional subspace, so that the high-dimensional raw data can be reconstructed from  $l$  low-dimensional space. The optimization objective of PCA is based on the mechanism of maximizing the variance after projections, which can be defined by

$$f_{PCA} = \arg \max_{V^T V=E} \sum_i^m \|V^T x_i - V^T u\|^2, \quad (1)$$

where  $m$  is the number of samples contained in the initial space,  $v$  is the projection vector of  $x_i$ , and  $u$  is the mean value of all samples, which can be written as

$$u = \frac{1}{m} \sum_{i=1}^m x_i, \quad (2)$$

However, PCA is a linear dimensionality reduction algorithm, so it possibly leads to poor performance when dealing with nonlinear data. Prates et al. [39] solved this problem by introducing Kernel hierarchical PCA, through which the dimensionality reduction of the nonlinear data is achieved.

(2) **Linear Discriminant Analysis (LDA)** [14] focuses on extracting the classification information and compressing the dimension of feature space when projecting high-dimensional samples into the optimal discriminant vector space. Samples in the new hyperplanes present the largest between-class distance and smallest within-class distance. Generally, the between-class scatter matrix  $S_B$  and the within-class scatter matrix  $S_W$  are defined as

$$S_B = \sum_{k=1}^C x_k (u_k - u)(u_k - u)^T, \quad (3)$$

$$S_W = \sum_{k=1}^C \sum_{j=1}^{x_k} ((u_{kj} - u_k)(u_{kj} - u_k)^T), \quad (4)$$

where  $C$  is the number of classes,  $x_k$  is the number of samples in the class  $k$ ,  $u_k$  is the sample mean of the class  $k$ ,  $u$  is the mean of all samples, and  $u_{ki}$  is the  $j^{th}$  sample in the class  $k$ . Thus, the final objective function of LDA can be written as

$$\arg \max \frac{tr(S_B)}{tr(S_W)}. \quad (5)$$

In contrast with PCA, linear discriminant analysis utilizes the prior knowledge of classes, so it can be used for dimensionality reduction and classification.

### 5.1.2 Local dimensionality reduction

Local dimensionality reduction aims to replace the global nonlinear relationship with a linear relationship in the local neighborhood, and each sample can be linearly reconstructed according to its local neighbors.

**1) Locally Linear Embedding (LLE)** [40] based on the embedding theory, seeks a mapping to transform data from a high-dimensional space to a low-dimensional space and then reconstructs a subspace by ensuring its neighborhood relationship, in which these subspaces still maintain such a linear relationship when embedded in the low-dimensional space. Considering an arbitrary measurement  $x_i$  and its  $K$  nearest neighbors  $x_{i_1}, \dots, x_{i_k}$ , the reconstruction error is

$$\arg \min \varepsilon(W) = \sum_{i=1}^n \|x_i - \sum_{j=1}^k W_{ij} x_{ij}\|^2, \quad (6)$$

where  $W_{ij}$  is the reconstruction coefficient of  $k$ -dimensional vectors and reflects the linear relationship between  $x_i$  and  $x_j$ , with the sum-to-one constraint:  $\sum_{j=1}^k W_{ij} = 1$ . Each local geometry seeks a low dimensional embedding from a high dimension, so the loss function can be reformulated as

$$\arg \min \varepsilon(Y) = \sum_{i=1}^n \|y_i - \sum_{j=1}^k W_{ij} y_j\|^2 = \|Y(I - W)\|^2 = \text{tr}(YMY^T), \quad (7)$$

where  $y_i$  is the low-dimensional representation of  $x_i$ ,  $W$  is the weight coefficient,  $M = (I - W)^T(I - W)$ , and  $Y$  is the low-dimensional global data.

LLE selects the measurements of neighbors, which makes the matrix sparse, thus reducing the time and space complexity and avoiding large dynamic optimization. However, it will necessarily involve the local minimum problem. In recent years, researchers have proposed improvements on this issue [44], including robust locally linear embedding (RLLE) [20] developed to deal with anomalies.

**2) Laplacian eigenmaps/locality preserving projections (LE/LPP)** [6, 17] preserve proximity relationships of measurements in the low-dimensional space by building an undirected weighted graph [33]. Before these manipulations, the similarity of the measurements should be determined. Usually, the Gaussian function is chosen as a similarity function

$$W(x_i, x_j) = \exp\left(-\frac{\|x_i - x_j\|^2}{2\sigma^2}\right), \quad (8)$$

Then LE/LPP project the measurements into the low-dimensional space and preserve the local geometry in the high-dimensional space. The objective function is

$$\arg \min \sum_{i=1}^n \sum_{j=1}^k \|y_i - y_j\|^2 W(x_i, x_j), \quad (9)$$

We can construct the Laplacian matrix  $L$  to solve the optimization problems, and  $L = D - W$ , where  $D$  is the diagonal weighting matrix of this undirected weighted graph. The generalized eigenvalue decomposition of LE is  $L\alpha = \lambda D\alpha$ , and LPP is  $YLY^T L\alpha = \lambda XDX^T\alpha$ .

LE/LPP preserve the local geometry in the high dimension. Therefore, the neighborhood search in the low dimension can obtain the search results similar to those in the high dimension. Since LE is nonlinear, it is insensitive to neighbor relationships. Luckily, Liu et al. [31] recently proposed local linear Laplacian eigenmaps to address this problem.

**3) Rank preserving discriminant analysis (RPDA)** [47] aims at solving the small sample learning problem in high-dimensional space. Different from traditional supervised dimensionality reduction algorithms, RPDA introduces a distance penalty factor to deal with the measurement concentration phenomenon, which can preserve within-class samples' rank order information on the local block as much as possible. However, it is worth noting that RPDA ignores rank order information and relatively extracts discriminant information of the between-class samples.

In RPDA, dimension reduction is performed according to the following two stages: part optimization and whole alignment. During the part optimization stage, a penalized factor is defined as

$$(w_i)_j = \begin{cases} \exp\left(-\|x_i - x_{i_j}\|^2/t\right), & \text{if } x_{i_j} \in N_{k_1}(x_i) \\ 0, & \text{otherwise,} \end{cases} \quad (10)$$

where  $x_i$  is the ranked closest within-class sample  $j$  with respect to sample  $i$ ,  $t$  is a parameter, and there exists a proportional relationship between  $t$  and the average distance of pairwise within-class samples.  $N_{k_1}(x_i)$  is the set of  $k_1$  closest within-class samples. Therefore, the differentiation of small distances in the initial distribution is emphasized with a large weighting, while that of large distances is emphasized with a small weighting. Then the entire objective function of part optimization is defined as

$$\arg \min_Y \text{intr}\left(YS_i L_i S_i^T Y^T\right), \quad (11)$$

where  $S_i \in R^{N \times (K+1)}$  is the selection matrix. By summarizing all the part optimizations, we can obtain the whole alignment

$$\begin{aligned} & \arg \min_Y \sum_{i=1}^N \text{tr}\left(YS_i L_i S_i^T Y^T\right) \\ &= \arg \min_Y \left(YL Y^T\right). \end{aligned} \quad (12)$$

Besides, to avoid the selection of parameter  $t$ , an alternative penalized factor is introduced

$$(w_i)_j = \begin{cases} \frac{x_i^T x_{i_j}}{\|x_i\| \cdot \|x_{i_j}\|} & \text{if } x_{i_j} \in N_{k_1}(x_i); \\ 0 & \text{otherwise.} \end{cases} \quad (13)$$

Therefore, the corresponding enhanced algorithm is named as RPDA.

## 5.2 Nearest neighbor classifier

In the experiment, we use the nearest neighbor (NN) algorithm [1] to classify sEMG signals. The principle of NN algorithm is to find the nearest sample in the feature space, so that the class of the new sample is consistent with the nearest sample. We choose Euclidean distance

as the measure of similarity between samples, which can be defined by:

$$D(x, y) = \sqrt{\sum_{k=1}^n (x_k - y_k)^2}, \quad (14)$$

where  $x$  and  $y$  represent two different samples,  $n$  is the sample data dimension, and  $x_k, y_k$  are the eigenvalues of  $x$  and  $y$  in  $k$  dimension.

### 5.3 Implementation details

In the proposed systematic experimental evaluation, we use fast Fourier transform (FFT) to extract the frequency-domain features of sEMG signal; because sEMG signal is a kind of time-series signal, it is difficult to preprocess in time domain. After conversion to frequency domain, noise can be easily filtered. Robust features were extracted to exploit the lower-limb sEMG activity in the following steps. First, corresponding to each axis (including x and y), the FFT coefficients were extracted using a 1000-point window, and there existed a 500-point overlap between consecutive windows. Second, we preserved the first 64 FFT coefficients for each sliding window, while the corresponding first DC component was discarded. Finally, the dataset was constructed, with each sample in the dataset containing 60,000 sample points in line with the 7616-dimensional FFT coefficients. It is worth noting that the feature sequence has a high dimension, and not all the features are useful, too high dimension will affect the computational efficiency, so we need to reduce the dimension.

In dimension reduction part, PCA is a nonparameter dimensionality reduction algorithm, and there is no subjective parameter intervention when performing dimensionality reduction on data. Other dimensionality reduction algorithms used in this article have hyperparameter settings that will affect the dimensionality reduction results, so we choose PCA as benchmark. We use PCA to reduce the dimension of the extracted features to 100 dimensions. Because we find that the top 100 dimensions feature after PCA dimensionality reduction account for 90% of the feature information. For LDA, LPP, LLE, and RPDA, we first utilized PCA to reduce the dimension of the extracted features to 200 dimensions, and then LDA, LPP, LLE, and RPDA were independently used to reduce the feature dimension to 100 dimensions. After dimension reduction, the activity recognition was performed based on NN classifier. We selected all movement samples of one person for testing, and the remaining samples as training sets to build a classifier model. Besides, to obtain a clearer explanation of the performance of each algorithm, we plotted the confusion matrix, which was corresponding to the optimal average recognition rate under each algorithm.

### 5.4 Results

We calculated the average recognition rate for different dimensions (1–100 dimensions) using varied algorithms of dimensionality reduction, as shown in Fig. 4. LDA had the lowest average recognition rate, but it performed best under the low-dimension ( $\leq 4$ ) condition. RPDA performed better than PCA and LLE when the dimension was lower than 36-dimensional. Nonetheless, the effectiveness of RPDA and LLE was worse than PCA with the increase of dimension. When the dimension number was larger than 36 dimensions, the performance of LPP achieved its best performance. In summary, LPP outperformed other dimensionality reduction algorithms as far as our dataset was concerned. Then, we reported the results of different activities via algorithms of dimensionality reduction. Table 5 shows the average

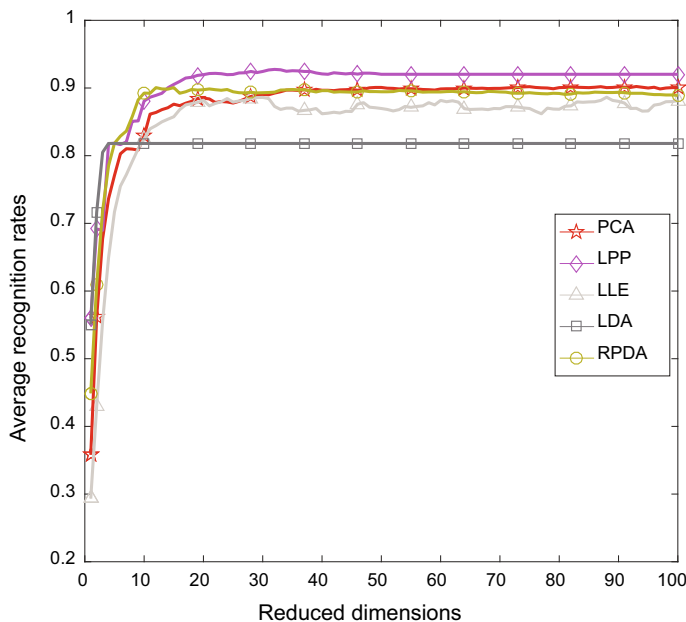


**Fig. 4** Average recognition rates using different dimensionality reduction algorithms in different dimensions

**Table 5** Average recognition rates of dimensionality reduction algorithms. (%)

Class	PCA (%)	LDA (%)	LLE (%)	LPP (%)	RPDA (%)
Jumping	87.22	77.92	88.33	90.00	85.14
Running	84.03	64.17	80.97	85.83	82.89
Standing	94.72	96.52	93.47	98.06	96.94
Walking	91.25	74.17	84.17	91.94	86.39
Lunge Stretching	93.89	96.25	96.25	97.92	98.89
Best Average Accuracy (Dimension)	90.22 (93)	81.806 (4)	88.64 (88)	92.75 (32)	90.06 (12)

recognition rates of five algorithms and the corresponding dimension of the best average recognition rate. The recognition rates of standing and lunge stretching exceeded those of other activities, as suggested in Table 5. In addition, Table 5 indicates that the best average recognition rates of PCA and RPDA differed by 0.16%, but that the dimensions retained by the two algorithms differed by 81 dimensions. Therefore, RPDA outperformed PCA in terms of storage saving.

In Table 6–9, we show the classification results of the data processed by each dimension reduction algorithm using the NN classification algorithm under different dimensions (1–40). It can be observed that PCA algorithm tends to be stable after 18 dimensions, and the accuracy is around 88.5%. Due to the limitation of LDA, it can get the best recognition accuracy in 4 dimensions, which is better than other algorithms in 4 dimensions. LLE tends to be stable after 20 dimensions, and the accuracy is around 88.19%. LPP algorithm tends to be stable after 21 dimensions, and the accuracy rate fluctuates around 92.13%, which is also the best of the five algorithms. RPDA algorithm tends to be stable after 10 dimensions, and the

**Table 6** The classification results of the sEMG data processed by each dimension reduction algorithm using the NN classification algorithm under different dimensions (1–10)

Dim.	1	2	3	4	5	6	7	8	9	10
PCA	0.3580	0.5613	0.6772	0.7363	0.7708	0.8027	0.8102	0.8097	0.8083	<b>0.8291</b>
LDA	0.5505	0.7163	0.8050	<b>0.8180</b>	0.8180	0.8180	0.8180	0.8180	0.8180	0.8180
LLE	0.2933	0.4294	0.5552	0.6491	0.7169	0.7550	0.7719	0.7913	0.8102	<b>0.8247</b>
LPP	0.5594	0.6916	0.6897	0.8177	0.8183	0.8163	0.8202	0.8508	0.8513	<b>0.8808</b>
RPDA	0.4488	0.6094	0.7183	0.7850	0.8183	0.8288	0.8363	0.8577	0.8825	<b>0.8925</b>

**Table 7** The classification results of the sEMG data processed by each dimension reduction algorithm using the NN classification algorithm under different dimensions (11–20)

Dim.	11	12	13	14	15	16	17	18	19	20
PCA	0.8613	0.8638	0.8680	0.8708	0.8761	0.8738	0.8775	0.8802	0.8844	<b>0.8850</b>
LDA	<b>0.8180</b>	0.8180	0.8180	0.8180	0.8180	0.8180	0.8180	0.8180	0.8180	0.8180
LLE	0.8397	0.8444	0.8500	0.8538	0.8575	0.8680	0.8750	0.8769	0.8786	<b>0.8819</b>
LPP	0.8863	0.8891	0.8922	0.9002	0.9052	0.9097	0.9147	0.9158	0.9186	<b>0.9197</b>
RPDA	0.8922	<b>0.9005</b>	0.8986	0.8983	0.9005	0.8922	0.8944	0.8977	0.8969	0.8975

**Table 8** The classification results of the sEMG data processed by each dimension reduction algorithm using the NN classification algorithm under different dimensions (21–30)

Dim.	21	22	23	24	25	26	27	28	29	30
PCA	0.8838	0.8786	0.8800	0.8794	0.8777	0.8802	0.8838	0.8875	0.8880	<b>0.8905</b>
LDA	<b>0.8180</b>	0.8180	0.8180	0.8180	0.8180	0.8180	0.8180	0.8180	0.8180	0.8180
LLE	0.8736	0.8772	0.8797	0.8844	0.8791	0.8808	0.8816	0.8847	0.8858	<b>0.8861</b>
LPP	0.9213	0.9216	0.9211	0.9197	0.9200	0.9222	0.9225	<b>0.9244</b>	0.9227	0.9244
RPDA	<b>0.8986</b>	0.8975	0.8966	0.8977	0.8944	0.8930	0.8927	0.8936	0.8927	0.8930

**Table 9** The classification results of the sEMG data processed by each dimension reduction algorithm using the NN classification algorithm under different dimensions (31–40)

Dim.	31	32	33	34	35	36	37	38	39	40
PCA	0.8900	0.8925	0.8944	0.8969	0.8969	0.8963	0.8975	0.8961	<b>0.8980</b>	0.8966
LDA	<b>0.8180</b>	0.8180	0.8180	0.8180	0.8180	0.8180	0.8180	0.8180	0.8180	0.8180
LLE	<b>0.8844</b>	0.8727	0.8683	0.8702	0.8702	0.8658	0.8669	0.8677	0.8697	0.8619
LPP	0.9266	<b>0.9275</b>	0.9269	0.9247	0.9255	0.9252	0.9244	0.9244	0.9222	0.9208
RPDA	0.8933	0.8938	0.8969	0.8972	<b>0.8977</b>	0.8972	0.8975	0.8958	0.8941	0.8961

accuracy is around 89.25%, which achieves higher accuracy than other algorithms with less dimension information. Figure 5 shows the confusion matrices corresponding to the highest action recognition accuracy of sEMG feature sequences processed by different dimensionality reduction algorithms. Among them, each column of confusion matrix represents the action prediction category, and the total number of each column represents the number of data

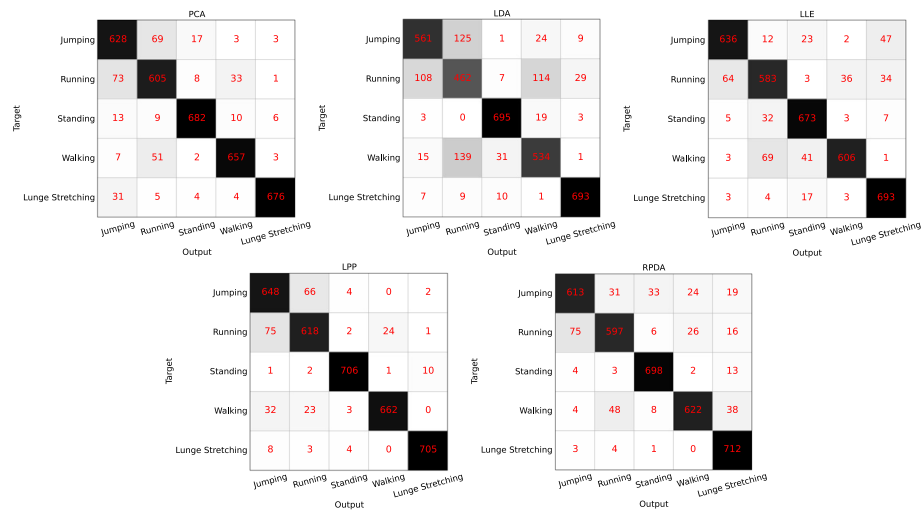


**Fig. 5** Classification confusion matrices of different algorithms

predicted as this kind of action; each row represents the real classification category, and the total number in each row represents the number of sEMG data instances of this category. The value on the diagonal of the matrix indicates the number of sEMG signals correctly classified. The darker the diagonal is, the better the effect of the dimension reduction algorithm is. The values of the remaining regions indicate the number of one type of sEMG signals that are mistakenly classified into other types of actions.

## 5.5 Discussion

LDA was a supervised dimensionality reduction algorithm, and the obtained dimension did not exceed C-1 dimension (C was the number of sample categories). Thus, after dimensionality reduction, LDA could not retain adequate information as much as possible. Therefore, when the subspace dimension increases, the above shortcoming seriously made LDA perform worse than PCA and other algorithms. Notably, since LPP was a supervised algorithm, it retained the local characteristics and discriminated between classes. We also observed the waveform of original signals and found that the waveform recognition of standing and lunge stretching was very high. Arguably, the more recognizable the waveform, the more conducive to classification. After the analysis of original waveforms, it was discovered that there existed approximation between the above activities, which reduced the performance of classification. From the perspective of muscle participation in movement, the muscle did not contract too much when a person was standing, and muscle tension only worked to maintain the standing posture, which also affected the performance of classification. Compared with standing, lunge stretching mainly stretched the high muscles, so it was easier to identify. However, because running and jumping were more intense than other activities, the degree and rhythm of muscle contraction performed more evidently. This was also another reason for confusion.

## 6 Conclusion

In this paper, we have presented a novel dataset for human activity recognition on lower-limb sEMG. The proposed HAR-sEMG dataset has a number of characteristics that are not present in previous sEMG datasets. First, the actions involved in our dataset design are common human activities. Second, considering the effects of different times on sEMG signals, our acquisition protocol has added the step of re-acquisition at an interval of 24 h. Third, our dataset has been collected over a sustained period of time, where each action has multiple sets of repetitions. In addition, this paper has also provided a scheme for recognizing human activities and exploiting high-dimensional sEMG signals and has given the evaluation results of the algorithm in this scheme. Furthermore, our evaluation system will serve as a guide to processing the high-dimensional signals for sEMG of HAR.

The lack of diversity in data collection is our limitation. In the future work, we will further expand the HAR-sEMG dataset, the data of different weather conditions and different age groups will be collected, we will also expand more actions and collect single joint motion data. In addition, the classification method based on deep learning will be used to recognize the sEMG signal, and the real-time prediction and recognition of human action based on sEMG signal will be realized.

**Acknowledgements** National Natural Science Foundation of China (61772508, U1713213), Shenzhen Technology Project (JCYJ20180507182610734, JCYJ20180302145648171), CAS Key Technology Talent Program, Yunnan Natural Science Funds under Grant 2018FY001(-013) and Grant 2019FA-045.

## References

1. Abeywickrama T, Cheema MA, Taniar D (2016) k-nearest neighbors on road networks: a journey in experimentation and in-memory implementation. *Proce Vldb Endow* 9(6):492–503
2. Ai H, Cheng X (2018) Research on embedded access control security system and face recognition system. *Measurement* 123:309–322
3. Al-Timemy, (2015) Improving the performance against force variation of emg controlled multifunctional upper-limb prostheses for transradial amputees. *IEEE Trans Neural Syst Rehabil Eng* 24(6):650–661
4. Atzori M, Gijsberts A, Kuzborskij I (2015) Characterization of a benchmark database for myoelectric movement classification. *IEEE Trans Neural Syst Rehabil Eng* 23(1):73–83
5. Atzori M, Gijsberts A, Heynen S, Building the Ninapro Database: A Resource for the Biorobotics Community. In Proceedings of the 4th IEEE RAS EMBS international conference on biomedical robotics and biomechatronics, pp 1258–1265 (2012)
6. Belkin M (2002) Laplacian eigenmaps and spectral techniques for embedding and clustering. *Adv Neural Inf Process Syst* 14(6):585–591
7. Bonomi A, Goris A, Yin B (2009) Detection of type, duration, and intensity of physical activity using an accelerometer. *Med Sci Sports Exercise* 41(9):1770–1777
8. Chaaraoui A, Florez-Revuelta F (2014) Adaptive human action recognition with an evolving bag of key poses. *IEEE Trans Auton Mental Develop* 6(2):139–152
9. Clancy E, Morin E, Merletti R (2002) Sampling, noisereduction and amplitude estimation issues in surface electromyography. *J Electromyogr Kinesiol* 12(1):1–16
10. Dua D, Graff C (2019) UCI Machine Learning Repository [<http://archive.ics.uci.edu/ml>]. Irvine, CA: University of California, School of Information and Computer Science
11. Du S, Vuskovic M, Temporal VS (2004) Spectral Approach to Feature Extraction from Prehensile EMG Signals. In Proceedings of the 2004 IEEE International Conference on Information Reuse and Integration, pp 344–350
12. Fathalla A, Salah A, Li K (2020) Deep end-to-end learning for price prediction of second-hand items. *Knowl Inf Syst* 62(4):4541–4568
13. Feng N, Shi Q, Wang H (2018) A soft robotic hand: design, analysis, sEMG control, and experiment. *Int J Adv Manufact Technol* 97(1–4):319–333
14. Fisher R (1936) The use of multiple measurements in taxonomic problems. *Ann Eugen* 7(2):179–188

15. Gao N, Zhao L (2016) A Pedestrian Dead Reckoning system using sEMG based on activities recognition. In: 2016 IEEE Chinese Guidance, Navigation and Control Conference 2361–2365
16. Hasic F, Corea C, Blatt J (2020) Decision model change patterns for dynamic system evolution. *Knowl Inf Syst*
17. He X, Niyogi P (2003) Locality preserving projections. *Adv Neural Inf Process Syst* 16(1):186–197
18. Hermens H, Freriks B, Disselhorstklug C (2000) Development of recommendations for sEMG sensors and sensor placement procedures. *J Electromyogr Kinesiol* 10(5):361–374
19. Hernandez F, Suarez L, Villamizar J (2019) Human Activity Recognition on Smartphones Using a Bidirectional LSTM Network, 2019 XXII Symposium on Image, Signal Processing and Artificial Vision
20. Hong C, Yeung D (2006) Robust locally linear embedding. *Pattern Recognit* 39(6):1053–1065
21. 3D body. Available: <https://www.3dbody.cn/>
22. Jalal A, Quaid M, Hasan A (2018) Wearable Sensor-Based Human Behavior Understanding and Recognition in Daily Life for Smart Environments. In: IEEE Conference on International Conference on Frontiers of information technology,
23. Jie L, Qiao L, Xinhui S (2019) Action parsing driven video summarization based on reinforcement learning. *IEEE Trans Circuits Syst Video Technol* 29(7):2126–2137
24. Jun-Young J, Wonho H, Hyundae Y (2015) A neural network-based gait phaseclassification method using sensors equipped on lower limb exoskeleton robots. *Sensors* 15(11):27738–27759
25. Kase N, Babaee M, Rigoll G (2017) Multi-view Human Activity Recognition Using Motion Frequency. *Image Processing*, pp 3963–3967
26. Khushaba R, Kodagoda S, Takruri M (2012) Toward improved control of prosthetic fingers using surface electromyogram (EMG) signals. *Expert Syst Appl* 39(12):10731–10738
27. Khushaba R, Kodagoda S, Liu D (2013) Muscle computer interfaces for driver distraction reduction. *Comput Methods Programs Biomed* 110(2):137–149
28. Krasoulis A, Kyranou I, Erden M (2017) Improved prosthetic hand control with concurrent use of myoelectric and inertial measurements. *J NeuroEng Rehabil* 14(1):71
29. Kwapisz J, Weiss G, Moore S (2010) Activity recognition using cell phone accelerometers. *ACM SIGKDD Explor Newslett* 12(2):74–82
30. Lee S, Yoon S, Cho H (2017) Human Activity Recognition from Accelerometer Data Using Convolutional Neural Network. *Big Data and Smart Computing*, pp 131–134
31. Liu F, Zhang W, Gu S (2016) Local linear laplacian eigenmaps: a direct extension of LLE. *Pattern Recognit Lett* 75:30–35
32. Lu J, Tong K (2019) Robust single accelerometer-based activity recognition using modified recurrence plot. *IEEE Sensors* 19(15):6317–6324
33. Luxburg U (2007) A tutorial on spectral clustering. *Statist Comput* 17(4):395–416
34. Morel J, Chenu C, Lorenz K (2015) Ecosystem services provided by soils of urban, industrial, traffic, mining, and military areas. *J Soils Sediments* 15(8):1659–1666
35. Nurhanim K, Elamvazuthi I, Izhar L (2017) Classification of human activity based on smartphone inertial sensor using support vector machine. *Robotics and manufacturing automation (ROMA)*, pp 1–5
36. Park S, Lee D, Chung WK (2019) Hierarchical motion segmentation through sEMG for continuous lower limb motions. *IEEE Robot Autom Lett* 99:1–1
37. Paul RJ (2010) What an information system is, and why is it important to know this. Iti international conference on information technology interfaces
38. Pizzolato S, Tagliapietra L, Cognolato M (2017) Comparison of six electromyography acquisition setups on hand movement classification tasks. *PLoS ONE* 12(10):e0186132
39. Prates R, Schwartz W (2016) Kernel Hierarchical PCA for Person Re-identification. International Conference on Pattern Recognition, pp 2091–2096
40. Roweis S, Saul L (2000) Nonlinear dimensionality reduction by locally linear embedding. *Science* 290(5500):2323–2326
41. Ryu J, Ryu J, Ryu J (2017) sEMG signal-based lower limb human motion detection using a top and slope feature extraction algorithm. *IEEE Signal Process Lett* 24:929–932932
42. Sapsanis C (2018) Recognition of basic hand movements using electromyography, [arXiv:1810.10062](https://arxiv.org/abs/1810.10062)
43. Sapsanis C, Georgoulas G, Tzes A (2013) Improving EMG based classification of basic hand movements using EMD. In: 2013 35th Annual International Conference of the IEEE Engineering in Medicine and Biology Society, pp 5754–5757
44. Shen Y, Pham NH, Xiao X (2016) Dynamic socialized gaussian process models for human behavior prediction in a health social network. *Knowl Inf Syst* 49(2):455–479
45. Shi X, Qin P, Zhu J (2020) Feature extraction and classification of lower limb motion based on sEMG signals. *IEEE Access* 99:1–1

46. Szabó C, Morgan L, Karkar K (2015) Electromyography-based seizure detector: preliminary results comparing a generalized tonic-clonic seizure detection algorithm to video-EEG recordings. *Epilepsia* 56(9):1432–1437
47. Tao D, Jin L, Wang Y (2014) Rank preserving discriminant analysis for human behavior recognition on wireless sensor networks. *IEEE Trans Ind Inf* 10(1):813–823
48. Tenenbaum J, Silva V, Langford J (2000) A global geometric framework for nonlinear dimensionality reduction. *Science* 290(5500):2319–2323
49. Theodoridis T, Agapitos A, Hu H (2011) A gaussian groundplan projection area model for evolving probabilistic classifiers. In: 13th annual genetic and evolutionary computation conference, pp 1339–1346
50. Toch E, Lerner B, Ben-Zion E (2019) Analyzing large-scale human mobility data: a survey of machine learning methods and applications. *Knowl Inf Syst* 58(3):501–523
51. Umakanthan S, Denman S, Fookes C (2014) Multiple Instance Dictionary Learning for Activity Representation. *Pattern Recognition*, pp 1377–1382
52. Vemulapalli R, Arrate F, Chellappa R (2014) Human action recognition by representing 3d skeletons as points in a lie group. *Computer Vision and Pattern Recognition* 588–595
53. Wei W, Wong Y, Du Y (2017) A multi-stream convolutional neural network for sEMG-based gesture recognition in muscle-computer interface. *Pattern Recognit Lett*
54. Wold S (1987) Principal component analysis. *Chemometr Intell Lab Syst* 2(1):37–52
55. Wu J, Tian Z, Sun L (2015) Real-time american sign language recognition using wrist-worn motion and sEMG sensors. In: International conference on wearable and implantable body sensor networks, pp 1–6
56. Xugang X, Minyan T, Miran S (2017) Evaluation of feature extraction and recognition for activity monitoring and fall detection based on wearable sEMG sensors. *Sensors* 17(6):1229
57. Yu Y, Fan L, Kuang S (2015) The research of sEMG movement pattern classification based on multiple fused wavelet function. In: IEEE International Conference on Cyber Technology in Automation IEEE
58. Zhang Z, Sup F (2014) Activity recognition of the torso based on surface electromyography for exoskeleton control. *Biomed Signal Process Control* 10:281–288
59. Zhang H, Yoshie O (2012) Improving human activity recognition using subspace clustering. *Mach Learn Cybren* 3:1058–1063
60. Zhang S, Zhang W, Niu J (2018) Improving short-text representation in convolutional networks by dependency parsing. *Knowl Inf Syst* 61:463–484
61. Zhu Z, Mingyao Z, Qi G (2019) A phase congruency and local laplacian energy based multi-modality medical image fusion method. *IEEE Access* 20811–20824
62. Zhu Z, Yin H, Chai Y (2018) A novel multi-modality image fusion method based on image decomposition and sparse representation. *Information Sciences*, pp 516–529

**Publisher's Note** Springer Nature remains neutral with regard to jurisdictional claims in published maps and institutional affiliations.



**Yu Luan** received a Master's degree in College of Control Theory and Control Engineering from Xi'an Jiaotong University, Xi'an, China. She is currently an Engineer of Instrument Control. Nowadays, her research interests include main control room, human-machine interfaces and human factor engineering.



**Yuhang Shi** received a B.E. degree in School of Information Science and Engineering from Yunnan University, China. He is now studying for a Master's degree. Nowadays, his research interests include human motion recognition and human -machine interface.



**Wanyin Wu** received a Master's degree in School of Information Science and Engineering, Yunnan University, Kunming, 650091, Yunnan, China. She is with Union Vision Innovation Science and Technology Ltd., Shenzhen, 518055, China.



**Zhiyao Liu** received a B.E. degree in College of Automation from Shanghai Jiao Tong University, China. He is currently a Senior Engineer of Instrument Control. Nowadays, his research interests include main control room and human -machine interface.



**Hai Chang** received a Master's degree in China Institute of Atomic Energy, Beijing, China. He is currently a Senior Engineer of human -machine interface design. Nowadays, his research interests include human -machine interface.



**Jun Cheng** received the B.Eng. and M.Eng. degrees from the University of Science and Technology of China, Hefei, China, in 1999 and 2002, respectively, and the Ph.D. degree from the Chinese University of Hong Kong in 2006. He is currently a Professor with the Shenzhen Institute of Advanced Technology, Chinese Academy of Sciences, Shenzhen, China, where he is also the Director of the Laboratory for Human Machine Control. His current research interests include computer vision, robotics, machine intelligence, and control.

## Authors and Affiliations

**Yu Luan<sup>1</sup> · Yuhang Shi<sup>3</sup> · Wanyin Wu<sup>4</sup> · Zhiyao Liu<sup>1</sup> · Hai Chang<sup>1</sup> · Jun Cheng<sup>2,5</sup> **

✉ Jun Cheng  
jun.cheng@siat.ac.cn

Yu Luan  
luanyu@cgnpc.com.cn

Yuhang Shi  
1037222866@qq.com

Wanyin Wu  
guquewan@gmail.com

Zhiyao Liu  
liuzhiyao@cgnpc.com.cn

Hai Chang  
changhai@cgnpc.com.cn

<sup>1</sup> State Key Laboratory of Nuclear Power Safety Monitoring Technology and Equipment, China Nuclear Power Engineering Co., Ltd., Shenzhen 518172, China

- 
- 2 Guangdong-Hong Kong-Macao Joint Laboratory of Human-Machine Intelligence-Synergy Systems, Shenzhen Institute of Advanced Technology, Chinese Academy of Sciences, Shenzhen 518055, China
  - 3 the FIST LAB, School of Information Science and Engineering, Yunnan University, Kunming 650091, Yunnan, China
  - 4 Union Vision Innovation Science and Technology Ltd., Shenzhen 518055, China
  - 5 The Chinese University of Hong Kong, Hong Kong, China